AAS 06-113

SYMPLECTIC ATTITUDE ESTIMATION FOR SMALL SATELLITES

James M. Valpiani*† & Philip L. Palmer‡

In this paper, a novel method for efficient high-accuracy satellite attitude estimation is presented. Symplectic numerical methods are applied to the Extended Kalman Filter (EKF) algorithm to give the SKF, which outperforms the standard EKF in the presence of nonlinearity and low measurement noise in the 1-D case. Building on this result, a six-state SKF is compared to an EKF of the same order for satellite attitude estimation. Simulation of a standard small satellite mission demonstrates orders of magnitude improvement in state accuracy and preservation of constants of motion. This new method shows promise for improved attitude estimation onboard resource-constrained small satellites.

INTRODUCTION

Increasing satellite attitude requirements demand high accuracy estimation methods capable of operating under significant computational constraints. To meet these demands, dynamical modeling has been used as an effective alternative to costly and resource intensive ADCS hardware for small satellite missions. However, these models have generally been propagated using methods ill-suited to take advantage of the unique properties of Hamiltonian systems.

Recently developed symplectic numerical methods have demonstrated promising results when applied to satellite attitude propagation. Symplectic methods inherently preserve the energy of Hamiltonian systems and as a result they have demonstrated increased stability and improved long-term performance in comparison to

*PhD Candidate, Surrey Space Centre, University of Surrey, j.valpiani@surrey.ac.uk

†The views expressed in this article are those of the author and do not reflect the official policy or position of the United States Air Force, Department of Defense, or the U.S. Government.

‡Reader, Surrey Space Centre, University of Surrey, p.palmer@surrey.ac.uk

nonsymplectic methods (such as Runge-Kutta). The result is a dramatic improvement in state propagation accuracy and constants of motion preservation even for symplectic methods inferior in order to nonsymplectic ones. Consequently, they are well suited for systems where preservation of conserved quantities is important for accurate predictions.

Motivated by a need for highly accurate and efficient attitude estimation algorithms, this paper presents a novel solution that capitalizes on the strengths of symplectic methods. Beginning with the 1-D case, a symplectic propagator is combined with Extended Kalman Filter (EKF) equations to give a symplectic Kalman Filter (SKF). The SKF's improved performance over the EKF in the presence of nonlinearity and low measurement noise motivates the development of a six-state SKF algorithm for satellite attitude estimation. Comparisons with a standard EKF demonstrate significantly better steady-state performance.

SYMPLECTIC NUMERICAL METHODS

A symplectic integrator is the exact solution to a discrete perturbed Hamiltonian system that is close to the actual Hamiltonian of interest. Because Hamiltonian systems have volume-preserving mappings in phase space as a consequence of Liouville's Theorem, symplectic integrators also preserve volume in phase space to within machine precision. Therefore, trajectories modeled by these integrators do not cross in phase space and energy errors about the true energy are bounded. Practically speaking, symplectic integrators preserve the invariants of motion for Hamiltonian systems to a much higher degree of accuracy than non-symplectic methods of the same order. When applied to satellite motion which is governed by rigid body dynamics, symplectic methods exactly conserve angular momentum and rotational energy with low amplitude sinusoidal variation and no numerical dissipation.

Generally, non-symplectic methods will introduce secular errors into conserved values with each evaluation and therefore misrepresent the conservative system as a dissipative one. Over time, the effect of this dissipation can significantly degrade state accuracy. In contrast, symplectic integrators' unique properties enable them to achieve state accuracies equivalent to nonsymplectic integrators while requiring less function evaluations (i.e. larger time steps) to do so. This makes them ideally suited to model Hamiltonian systems such as satellite attitude, particularly onboard satellites with constrained computational resources. When computational resources are not a significant concern, the comparatively higher-accuracy solutions of symplectic integrators reduce the requirement for frequent measurement updates in the attitude estimation problem.

Recently, symplectic methods have been applied in a wide variety of fields, ranging from chemistry to celestial mechanics.[1] However, these methods have generally been limited to stochastic applications where the behavior of a multi-body system

is of greater concern than the behavior of any particular system component.[2] Conventional wisdom held that symplectic methods would not be useful for modeling specific trajectories.[3,4]

This was dispelled by Palmer et al[5] in 1999, when they published an orbit estimation algorithm that used symplectic methods for modeling individual satellite orbits. Motivated by the relatively high power consumption of GPS receivers onboard small satellites, the authors developed a method that was both fast and highly accurate to minimize CPU power consumption and reduce the number of GPS measurements required for orbit determination. Using symplectic methods, they demonstrated modeling accuracies on the order of centimeters for propagations spanning multiple days with sparse measurements.

The application of symplectic numerical methods to satellite ADCS design is a very recent development. In 2004, the same authors presented results from the first application of symplectic methods to satellite attitude propagation.[6] The authors sought to address the drawbacks incurred from linearization inherent in the EKF approach to small satellite attitude estimation, including: shorter timesteps and increased computational demand needed to limit error growth in simplified state prediction methods; limited ability to utilize more accurate integration schemes due to constrained computer resources; and increased polling of attitude sensors in order to compensate. Noting the predictability of small satellite dynamics and the small disturbances they experience, the authors pointed out that symplectic methods are well-suited for attitude propagation. Using a simple low-order composite symplectic method and a time-transformation, they propagated torque-free satellite motion while conserving integrals of motion exactly. In the presence of gravity-gradient torque, the authors demonstrated low amplitude sinusoidal errors about conserved system values using large timesteps; in contrast, a standard nonsymplectic Runge-Kutta method gave secularly increasing errors of the same order of magnitude using a stepsize two orders of magnitude smaller.

1-D SYMPLECTIC KALMAN FILTER

Based on the advantages of using symplectic numerical methods outlined above, it seemed reasonable to hypothesize that they provide improved accuracy when applied to nonlinear estimation for Hamiltonian systems. In order to test this hypothesis and determine the advantages and disadvantages of this approach, the application of symplectic propagation to nonlinear estimation in the 1-D case was investigated.

1-D EQUATIONS OF MOTION

Starting with the equations for a nonlinear pendulum

$$H = \frac{1}{2}p^2 - \Omega^2 \cos(q) \tag{1a}$$

$$\dot{q} = p \tag{1b}$$

$$\dot{p} = -\Omega^2 \sin(q) \tag{1c}$$

a symplectic discretization was applied. The numerical method chosen was the second-order implicit midpoint rule (IMPR)[2]

$$z_{j+1} = z_j + \Delta t f\left(\frac{z_j + z_{j+1}}{2}\right) \tag{2}$$

where $f(z) = \frac{dz}{dt}$. Note that subscripts j are used to indicate propagation times. Applying the IMPR method to Equations (1) gives

$$q_{j+1} = 2X_{j+1} - q_j \tag{3a}$$

$$p_{j+1} = p_j - \Delta t \Omega^2 \sin(X_{j+1}) \tag{3b}$$

$$X_{j+1} = \frac{q_j + q_{j+1}}{2} \tag{3c}$$

$$X_{j+1} + \frac{\Delta t^2}{4}\Omega^2 \sin(X_{j+1}) = \frac{\Delta t}{2}p_j + q_j \tag{3d}$$

In this formulation, all system nonlinearity is contained in the variable X_{j+1} and the update equations for q_{j+1} and p_{j+1} are simple linear equations. The iterative Newton-Raphson method was employed to solve Equation (3d) to within a user-defined tolerance.

1-D SYMPLECTIC KALMAN FILTER EQUATIONS

The well-known Extended Kalman Filter algorithm is summarized below. Note that the subscripts n are used to indicate observation times:

- Propagate the previous time's state estimate $\hat{\mathbf{x}}_{n-1}$ to obtain the current time's state prediction $\hat{\mathbf{x}}_n^-$

$$\hat{\mathbf{x}}_n^- = \hat{\mathbf{x}}_{n-1} + \int_{t_{n-1}}^{t_n} f(\hat{\mathbf{x}}_{n-1})\, dt \tag{4}$$

- Propagate the previous time's error covariance estimate P_{n-1} to obtain the current time's error covariance prediction P_n^- using the state transition matrix Φ_n and process noise Q_n

$$P_n^- = \Phi_n P_{n-1} \Phi_n^T + Q_n \tag{5}$$

- Calculate the Kalman gain K_n using the observation matrix H_n and the observation noise covariance R_n

$$K_n = P_n^- H_n^T \left(H_n P_n^- H_n^T + R_n \right)^{-1} \tag{6}$$

- Calculate the current state estimate $\hat{\mathbf{x}}_n$

$$\hat{\mathbf{x}}_n = \hat{\mathbf{x}}_n^- + K_n \left(\mathbf{z}_n - H_n \hat{\mathbf{x}}_n^- \right) \tag{7}$$

- Calculate the current error covariance estimate P_n

$$P_n = \left(\mathrm{I} - K_n H_n \right) P_n^- \tag{8}$$

The standard EKF was implemented using a second-order nonsymplectic Runge-Kutta numerical method[7] for state propagation in Equation (4). The symplectic EKF (hereafter referred to as SKF) was created using Equations (3) for state propagation.

MONTE CARLO SIMULATION SETUP

In order to compare the performance of the EKF and the SKF, a Monte Carlo simulation was developed using the following conditions:

- State vector composed of generalized coordinate, q, and generalized momentum, p

$$\mathbf{x} = [q \;\; p]^T \tag{9}$$

- Direct observation of q

$$H = [1 \;\; 0] \tag{10}$$

- Approximate integration of the state transition matrix

$$\Phi = \mathrm{I}_{2x2} + \begin{bmatrix} \frac{\partial \dot{q}}{\partial q} & \frac{\partial \dot{q}}{\partial p} \\ \frac{\partial \dot{p}}{\partial q} & \frac{\partial \dot{p}}{\partial p} \end{bmatrix} \Delta t \tag{11}$$

- Following the standard practice for comparing estimators set by Athans,[8,9,10] process noise was omitted to prevent masking of linearization errors

$$Q = 0_{2x2} \tag{12}$$

To determine the relative merits of the SKF versus the EKF, the simulation varied over a set of parameters as outlined in Table 1.

Nonlinearity (q_0, rad)	Measurement Noise Variance (R, rad^2)	Measurements/Orbit
1.29	$(5 * 10^{-5})^2$	400
1.86	$(5 * 10^{-4})^2$	200
2.44	$(5 * 10^{-3})^2$	100
2.73	$(5 * 10^{-2})^2$	50
3.14	$(5 * 10^{-1})^2$	10

Table 1: 1-D Monte Carlo Simulation Parameter Space

The expected performance of both filters decreased down each column in Table 1, with the pathological parameter set defined by the bottom row. For each of the 125 possible combinations of parameters, 25 Monte Carlo runs were conducted. Each run used unique observation sets defined by $Z_{run} = \{z_n : t_0 < t_n \leq t_{end}\}$ where $z_n = q_n + v_n$ and $v_n \sim N(0, R_{parameter\ set})$. In addition, parameters that were constant for both the EKF and SKF throughout the simulation are outlined in Table 2.

Propagation Δt (sec)	Truth Δt (sec)	P_0 $\left(\text{rad}^2, \frac{\text{rad}^2}{\text{sec}^2}\right)$	Ω^2	IMPR Tolerance (rad)
$5 * 10^{-3}$	$5 * 10^{-5}$	$\begin{bmatrix} 1 & 0 \\ 0 & 1 \end{bmatrix}$	1	$1 * 10^{-12}$

Table 2: 1-D Monte Carlo Simulation Constant Parameters

Truth Δt was the propagation step used for determining the true values of the pendulum state and IMPR Tolerance was the value used in the Newton-Raphson method for Equation (3d). Since only steady-state performance was evaluated, P_0 was kept constant and artificially large to ensure initial filter convergence.

MONTE CARLO SIMULATION RESULTS

For each parameter set, the absolute value of the position error was averaged across the 25 runs at each observation time. The results from the filters within each parameter set fell into one of four categories: the filter converged, the filter diverged, the filter failed to reach steady-state and had unbounded error growth at the end of the simulation, or the filter reached steady-state with errors greater than 3 σ of the measurement noise. For this system, 99.73% of the observations are within 3 σ of the true value;[11] subsequently, results with steady-state errors greater than this value, results with unbounded error growth, and divergent results were grouped together as undesirable filter results. Then, a visualization tool was used to make general trend observations regarding the performance of each filter as different parameters varied; results are shown in Figure 1. These visualizations are useful for developing an intuitive feel for the filters' relative performance trends. Comparing the two visualizations, it appears that the SKF gives convergent behavior in regions of high nonlinearity, high measurement frequency, and low measurement noise whereas the

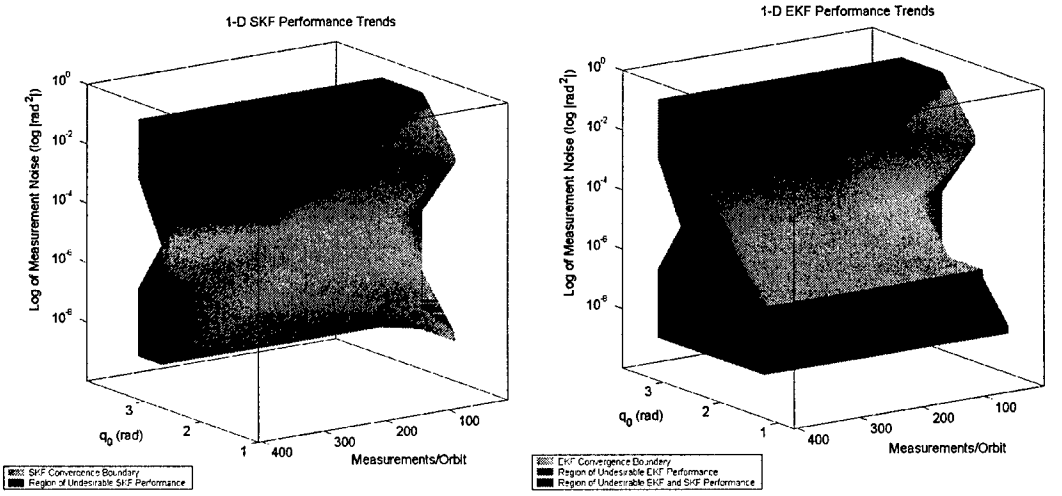

Figure 1: Comparison of 1-D SKF and EKF Performance Trends

EKF appears to fall short in these areas. In the EKF region of undesirable performance (red volume), the ratio of the position error below which the filters performed for 95% of the steady-state gave a relative measure of the advantage of using the SKF in lieu of the EKF. For example, Figure 2 shows the effect of reducing the measurement noise standard deviation by an order of magnitude from the left plot to the right: the ratio of the 95% steady-state error value increases nearly tenfold. Though these ratios are meaningless as independent measures of performance (due to the divergent nature of the EKF solution), they demonstrate the advantage of using the SKF as measurement noise decreases. Similar relationships hold for increasing nonlinearity and increasing measurement frequency; these results indicate that the SKF is more suited than the EKF to handle nonlinear Hamiltonian systems in the presence of high-accuracy, high-frequency observations.

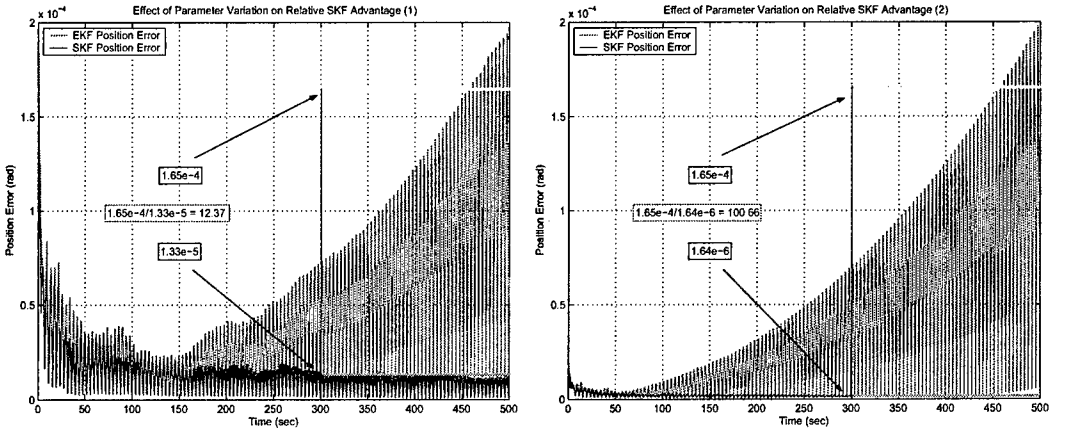

Figure 2: Effect of Parameter Variation on Relative SKF Advantage

SYMPLECTIC KALMAN FILTER FOR SATELLITE ATTITUDE

Building on the results from the 1-D case, a symplectic propagator was developed based on previous work by Palmer[6,12,13] and incorporated into a six-state SKF. Then, comparisons to a nonsymplectic flight-tested EKF used on current and previous SSTL missions[14,15] were made.

SATELLITE ATTITUDE PROBLEM

Fundamentally, the problem of three-axis attitude parameterization is to specify the orientation of the satellite body frame with respect to another known coordinate frame (commonly, the local orbital or inertial coordinate frames). Euler angles offer an intuitive way to represent a satellite's attitude. These angles are determined from a series of positive right-hand rotations from the local orbital coordinate frame to the satellite body frame. In this paper, the pitch-roll-yaw (2-1-3) sequence is used. However, though Euler angles are particularly useful due to their convenient physical interpretation, there are no all-attitude 3-parameter sets that are free of singularities.[16] As a result, it is often convenient to utilize the singularity-free Euler parameters in attitude equations, represented in this paper by the 4-parameter quaternion $\mathbf{q}$.

DYNAMICS

Satellite dynamics in inertial space are governed by Euler's equations of motion. Describing the rotational motion of the satellite with respect to an inertial frame gives[17]

$$I\dot{\boldsymbol{\omega}}_{b/i} = -\boldsymbol{\omega}_{b/i} \times \left(I\boldsymbol{\omega}_{b/i} + \mathbf{h}\right) - \dot{\mathbf{h}} + \mathbf{N} \tag{13}$$

where

$$I = \begin{bmatrix} I_{11} & I_{12} & I_{13} \\ I_{21} & I_{22} & I_{23} \\ I_{31} & I_{32} & I_{33} \end{bmatrix} \tag{14}$$

is the moment of inertia tensor of the satellite,

$$\boldsymbol{\omega}_{b/i} = [\omega_1 \;\; \omega_2 \;\; \omega_3]^T \tag{15}$$

is the inertially referenced body angular rate vector,

$$\mathbf{h} = [h_1 \;\; h_2 \;\; h_3]^T \tag{16}$$

is the satellite's internal angular momentum vector (produced by reaction wheels or control-moment gyroscopes, for example), $\mathbf{N}$ is the total external torque vector about the satellite center of mass with respect to the inertial coordinate frame, and subscripts 1, 2, and 3 are the axes of the satellite body coordinate frame. Assuming the principal moments of inertia axes are along the body axes, the off-diagonal terms of Equation (14) are zero.

KINEMATICS

Kinematics, or the study of motion independent of forces, are governed by a separate equation based on quaternions. Assuming a satellite in a circular orbit, the quaternion evolution is[18]

$$\dot{\mathbf{q}} = \frac{1}{2}\left[\Omega\left(\mathbf{o}_1\right) - \Omega^*\left(\mathbf{o}_2\right)\right]\mathbf{q} \tag{17}$$

where $\mathbf{o}_1 = \begin{bmatrix}\boldsymbol{w}_{b/i}^T & 0\end{bmatrix}^T$, $\mathbf{o}_2 = [0 \;\; n \;\; 0 \;\; 0]^T$, n is the orbital mean motion, and

$$\begin{aligned}\mathbf{p} \otimes \mathbf{q} = \Omega\left(\mathbf{p}\right)\mathbf{q} &= \begin{bmatrix} p_4 & p_3 & -p_2 & p_1 \\ -p_3 & p_4 & p_1 & p_2 \\ p_2 & -p_1 & p_4 & p_3 \\ -p_1 & -p_2 & -p_3 & p_4 \end{bmatrix}\begin{bmatrix} q_1 \\ q_2 \\ q_3 \\ q_4 \end{bmatrix} \\ = \Omega^*\left(\mathbf{q}\right)\mathbf{p} &= \begin{bmatrix} q_4 & -q_3 & q_2 & q_1 \\ q_3 & q_4 & -q_1 & q_2 \\ -q_2 & q_1 & q_4 & q_3 \\ -q_1 & -q_2 & -q_3 & q_4 \end{bmatrix}\begin{bmatrix} p_1 \\ p_2 \\ p_3 \\ p_4 \end{bmatrix}\end{aligned} \tag{18}$$

SYMPLECTIC PROPAGATOR FOR SATELLITE ATTITUDE

Consider the case of a triaxial satellite in a circular orbit with mean motion n. Its rotational dynamics are governed by Equation (13) and its kinematics are governed by Equation (17). For the sake of convenience, $\boldsymbol{\omega}$ is taken to mean $\boldsymbol{\omega}_{b/i}$ (inertially referenced body angular rates) and motion is described with respect to the principal satellite axes I_1, I_2, and I_3. Assuming no external or internal torques (i.e. $\mathbf{N} = 0$ and $\dot{\mathbf{h}} = 0$), then the system is Hamiltonian and two conserved values of motion are the rotational energy

$$E = \frac{1}{2}\sum_{k=1}^{3}\omega_k I_k \omega_k \tag{19}$$

and the angular momentum of the satellite in the inertial frame

$$\mathbf{L} = D(nt)A^T(I\boldsymbol{\omega} + \mathbf{h}) \tag{20}$$

where A is the direction cosine matrix (DCM) from the local orbital frame to the body frame, and D is the DCM from the inertial frame to the local orbital frame. The symplectic IMPR method will exactly conserve these quadratic first integrals over time.[2] Applying the second-order IMPR method from Equation (2) to the satellite dynamics and using superscripts to denote propagation steps gives

$$\omega_1^{(j+1)} = \omega_1^{(j)} + \Delta t\left(\alpha_1\tilde{\omega}_2\tilde{\omega}_3 + H_{12}\tilde{\omega}_2 + H_{13}\tilde{\omega}_3 + u_1\right) \tag{21a}$$

$$\omega_2^{(j+1)} = \omega_2^{(j)} + \Delta t\left(\alpha_2\tilde{\omega}_1\tilde{\omega}_3 + H_{21}\tilde{\omega}_1 + H_{23}\tilde{\omega}_3 + u_2\right) \tag{21b}$$

$$\omega_3^{(j+1)} = \omega_3^{(j)} + \Delta t\left(\alpha_3\tilde{\omega}_1\tilde{\omega}_2 + H_{31}\tilde{\omega}_1 + H_{32}\tilde{\omega}_2 + u_3\right) \tag{21c}$$

where

$$u_k = \frac{N_k}{I_k},\ k = 1,2,3 \tag{22}$$

$$\tilde{\omega_k} = \frac{\omega_k^{(j)} + \omega_k^{(j+1)}}{2},\ k = 1,2,3 \tag{23}$$

$$\alpha_1 = \frac{I_2 - I_3}{I_1},\ \alpha_2 = \frac{I_3 - I_1}{I_2},\ \alpha_3 = \frac{I_1 - I_2}{I_3} \tag{24}$$

$$H_{12} = \frac{h_3}{I_1},\ H_{13} = \frac{h_2}{I_1},\ H_{21} = \frac{h_3}{I_2},\ H_{23} = -\frac{h_1}{I_2},\ H_{31} = -\frac{h_2}{I_3},\ H_{32} = \frac{h_1}{I_3} \tag{25}$$

Δt is the timestep, and superscripts (j) and $(j+1)$ indicate propagation steps. Once the dynamics are propagated to give the satellite angular velocity, the next step is to propagate the kinematics to determine the satellite attitude. Assuming that the angular velocity vector in body coordinates is constant over a single timestep, a closed-form solution to Equation (17) exists[19]

$$\mathbf{q}_{j+1} = e^{\frac{1}{2}\Delta t\Omega(\mathbf{o}_1)} e^{\frac{1}{2}\Delta t\Omega^*(\mathbf{o}_2)} \mathbf{q}_j \tag{26}$$

This solution can be treated via a two step method[6]

$$\mathbf{q}_s = e^{\frac{1}{2}\Delta t\Omega^*(\mathbf{o}_2)}\mathbf{q}_j = \cos\left(\frac{n\Delta t}{2}\right)\mathbf{q}_j + \frac{\sin\left(\frac{n\Delta t}{2}\right)}{n}\Omega^*(\mathbf{o}_2)\,\mathbf{q}_j \tag{27a}$$

$$\mathbf{q}_{j+1} = e^{\frac{1}{2}\Delta t\Omega(\mathbf{o}_1)}\mathbf{q}_s = \cos\left(\frac{|\boldsymbol{\omega}|\Delta t}{2}\right)\mathbf{q}_s + \frac{\sin\left(\frac{|\boldsymbol{\omega}|\Delta t}{2}\right)}{|\boldsymbol{\omega}|}\Omega(\mathbf{o}_1)\,\mathbf{q}_s \tag{27b}$$

The question now arises as to the relationship between the dynamics and the kinematics. In the case of a Hamiltonian system which can be separated naturally

$$H(q,p) = H_A(q,p) + H_B(q,p) \tag{28}$$

then different rules can be applied to each variable subset. This is the approach used in partitioned Runge-Kutta methods such as the second-order Störmer-Verlet (leapfrog) method[2,20]

$$q_{j+\frac{1}{2}} = f_1\left(q_j, \frac{\Delta t}{2}, \left.\frac{\partial H_A}{\partial p}\right|_{p=p_j}\right) \tag{29a}$$

$$p_{j+1} = f_2\left(p_j, \Delta t, \left.\frac{\partial H_B}{\partial q}\right|_{q=q_{j+\frac{1}{2}}}\right) \tag{29b}$$

$$q_{j+1} = f_1\left(q_{j+\frac{1}{2}}, \frac{\Delta t}{2}, \left.\frac{\partial H_A}{\partial p}\right|_{p=p_{j+1}}\right) \tag{29c}$$

where f_1 and f_2 refer to the specific method used to propagate each variable. Combining this leapfrog method with the propagation equations outlined above for the

dynamics and kinematics gives a composite numerical method for the satellite attitude, and every composite method is symplectic when applied to Hamiltonian equations.[21]

A number of other modifications to this model have been made but have not yet been included in this analysis. Though the IMPR discretization for the dynamics preserves the true phase space trajectory, a shift in phase along the trajectory is possible and a time transformation has been derived that accounts for the shifts.[13] Additionally, gravity gradient torques have been incorporated into the dynamical equations. Though angular momentum and rotational energy are no longer constants of motion, a Jacobi constant arises and it is preserved by the symplectic attitude propagator. In the future, other torques may be included in the dynamical model as perturbations, which has been done previously in symplectic orbit propagators.[21]

6-STATE KALMAN FILTER

The symplectic propagator described above was added to the flight-tested SSTL 6-state Kalman filter algorithm to determine the relative merits of the SKF over the EKF when applied to the satellite attitude problem. However, the use of quaternions for kinematic parameterization in the symplectic propagator presents a unique problem. Though quaternions are 4-parameter sets, they are not independent due to the unit norm constraint. It is therefore possible to estimate all four quaternion values, or to estimate three quaternion values and derive the fourth. Both methods have merits, but the three quaternion approach, known as the 6-state filter, is generally more computationally efficient.[22,23] The algorithm outlined below closely follows the SSTL derivation by Hashida.[24]

Assuming that the true state is a small deviation from the predicted state, error values can be defined based on these relationships

$$\mathbf{q} = \delta\mathbf{q} \otimes \hat{\mathbf{q}}^- \tag{30a}$$

$$\boldsymbol{\omega} = \delta\boldsymbol{\omega} + \hat{\boldsymbol{\omega}}^- \tag{30b}$$

where the $\hat{}$ subscript indicates a state estimate and the $^-$ subscript indicates that the estimate has been propagated forward in time to give a state prediction. In addition to the true 7-parameter state, $\mathbf{x} = \left[\mathbf{q}^T \ \boldsymbol{\omega}^T\right]^T$, the 6-parameter error state is defined as

$$\tilde{\mathbf{x}} = \left[\delta\vec{q}^T \ \delta\boldsymbol{\omega}^T\right]^T \tag{31}$$

where the $\tilde{}$ superscript denotes variables associated with the error state; $\delta\vec{q}$ is defined by $\delta\mathbf{q} = \left[\delta\vec{q}^T \ \delta q_4\right]^T$; and $\delta q_4 = +\sqrt{1 - |\delta\vec{q}|^2}$. Linearizing the dynamics and kinematics from Equations (13) and (17) and using the same assumptions from the

symplectic propagator gives

$$\delta\dot{\vec{q}} = -C\left(\hat{\boldsymbol{\omega}}\right)\delta\vec{q} + \frac{1}{2}\delta\boldsymbol{\omega} \tag{32a}$$

$$I\delta\dot{\boldsymbol{\omega}} = -\left[C\left(\hat{\boldsymbol{\omega}}\right)I - C\left(I\hat{\boldsymbol{\omega}} + \mathbf{h}\right)\right]\delta\boldsymbol{\omega} \tag{32b}$$

where

$$\mathbf{a} \times \mathbf{b} = C(\mathbf{a})\mathbf{b},\ C(\mathbf{a}) = \begin{bmatrix} 0 & -a_3 & a_2 \\ a_3 & 0 & -a_1 \\ -a_2 & a_1 & 0 \end{bmatrix} \tag{33}$$

These linearized equations are then used to form the state transition matrix for the error state

$$\tilde{\Phi}_n = \mathrm{I}_{6x6} + \tilde{F}_n\Delta t,\ \tilde{F}_n = \left.\frac{\partial\left(\delta\dot{\vec{q}}, \delta\dot{\boldsymbol{\omega}}\right)}{\partial\left(\delta\vec{q}, \delta\boldsymbol{\omega}\right)}\right|_n = \begin{bmatrix} -C\left(\hat{\boldsymbol{\omega}}_n\right) & \frac{1}{2}\mathrm{I}_{3x3} \\ 0_{3x3} & -I^{-1}\left[C\left(\hat{\boldsymbol{\omega}}_n\right)I - C\left(I\hat{\boldsymbol{\omega}}_n + \mathbf{h}_n\right)\right] \end{bmatrix} \tag{34}$$

In this implementation, direct observation of $\delta\vec{q}$ is assumed for simplification, giving the following observation matrix

$$\tilde{H} = \begin{bmatrix} \mathrm{I}_{3x3} & 0_{3x3} \end{bmatrix} \tag{35}$$

The 6-state Kalman Filter algorithm follows Equations (4) to (8), with some modifications:

- Calculate the current time's 7-parameter state prediction $\hat{\mathbf{x}}_n^- = \left[\hat{\mathbf{q}}_n^{-T}\ \hat{\boldsymbol{\omega}}_n^{-T}\right]^T$

$$\hat{\mathbf{x}}_n^- = \hat{\mathbf{x}}_{n-1} + \int_{t_{n-1}}^{t_n} f\left(\hat{\mathbf{x}}_{n-1}\right)dt \tag{36}$$

- Propagate the error state's error covariance matrix forward in time using the error state transition matrix in Equation (34)

$$\tilde{P}_n^- = \tilde{\Phi}_n\tilde{P}_{n-1}\tilde{\Phi}_n^T + \tilde{Q}_n \tag{37}$$

- Calculate the error Kalman gain

$$\tilde{K}_n = \tilde{P}_n^-\tilde{H}_n^T\left(\tilde{H}_n\tilde{P}_n^-\tilde{H}_n^T + R_n\right)^{-1} \tag{38}$$

- Calculate the error state estimate $\hat{\tilde{\mathbf{x}}}_n = \left[\delta\hat{\vec{q}}_n^T\ \delta\hat{\boldsymbol{\omega}}_n^T\right]^T$

$$\hat{\tilde{\mathbf{x}}}_n = \tilde{K}_n\left(\mathbf{z}_n - h\left(\hat{\mathbf{x}}_n^-\right)\right) \tag{39}$$

- Calculate the error state's error covariance matrix estimate

$$\tilde{P}_n = \left(\mathrm{I}_{6x6} - \tilde{K}_n\tilde{H}_n\right)\tilde{P}_n^- \tag{40}$$

- Calculate the 7-parameter state estimate $\hat{x}_n = \left[\hat{\mathbf{q}}_n^T \ \hat{\boldsymbol{\omega}}_n^T\right]^T$ using the error state estimate $\hat{\tilde{\mathbf{x}}}_n$, the 7-parameter state prediction $\hat{\mathbf{x}}_n^-$, and Equations (30)

$$\delta\hat{q}_4 = +\sqrt{1 - \left|\delta\hat{\vec{q}}_n\right|^2} \tag{41a}$$

$$\delta\hat{\mathbf{q}}_n = \left[\delta\hat{\vec{q}}_n^T \ \delta\hat{q}_4\right]^T \tag{41b}$$

$$\hat{\mathbf{q}}_n = \delta\hat{\mathbf{q}}_n \otimes \hat{\mathbf{q}}_n^- \tag{41c}$$

$$\hat{\boldsymbol{\omega}}_n = \delta\hat{\boldsymbol{\omega}}_n + \hat{\boldsymbol{\omega}}_n^- \tag{41d}$$

The standard 6-state EKF uses a second-order nonsymplectic Adams-Bashford method to propagate the state in Equation (36), while the SKF uses the symplectic propagator outlined previously.

SYMPLECTIC KALMAN FILTER RESULTS

To compare the two estimation methods, realistic satellite configurations and mission profiles were selected for simulation. Many configurations were tested, and a representative case was based on the upcoming U.S. Air Force Academy FalconSAT-3 small satellite mission,[25] with one modification. In order to test the findings of Section , a high-accuracy measurement device was substituted for the standard low-accuracy magnetometer planned for FalconSAT-3. Instead, the Advanced Stellar Compass (ASC)[26] recently flown on ESA's PROBA-1 mission was selected due to its successful implementation as a rate-gyro replacement onboard an agile resource-constrained small satellite, and for its ability to provide high-accuracy attitude observations with high frequency at fast rotation rates (up to 2.5 $\frac{\text{deg}}{\text{sec}}$). Table 3 summarizes the simulated satellite properties.

I (kgm^2)			Mass (kg)	Obs Freq (Hz)	Obs Accuracy (1 σ, arcsec)
3.89	0	0	50	2	1
0	3.89	0			
0	0	1.32			

Table 3: SKF Versus EKF Simulation Satellite Properties

In addition, properties for a circular orbit were derived from the FalconSAT-3 mission[27,28] and are summarized in Table 4.

Mean Motion ($\frac{\text{deg}}{\text{sec}}$)	Orbit Period (min)	Altitude (km)	Inclination (deg)
0.0627	95.7	560	35

Table 4: SKF Versus EKF Simulation Orbit Properties

An SSTL RK-45 integrator was used to propagate the satellite kinematic and dynamic equations to obtain both the true trajectory and the observation set using observation properties from Table 3 and initial conditions from Table 5.

q_1	q_2	q_3	q_4	w_1 $\left(\frac{\text{deg}}{\text{sec}}\right)$	w_2 $\left(\frac{\text{deg}}{\text{sec}}\right)$	w_3 $\left(\frac{\text{deg}}{\text{sec}}\right)$	Δt (sec)
0.0088	0.0086	0.0086	0.9999	2	0.3	0.5	0.01

Table 5: SKF Versus EKF Simulation Initial Conditions

For filter initialization, the diagonal values of the covariance matrix for both the EKF and SKF were set high relative to the measurement noise since only steady state performance was considered. Measurement noise was selected to give optimal filter performance and process noise was set to zero to minimize masking of linearization errors, consistent with previous authors' analysis.[8,17] The state vector for both filters was initialized to zero values, and a standard small satellite ADCS step size of 0.1 seconds was used. In Figure 3, the significant difference between the two filters' state estimation performances can be seen.

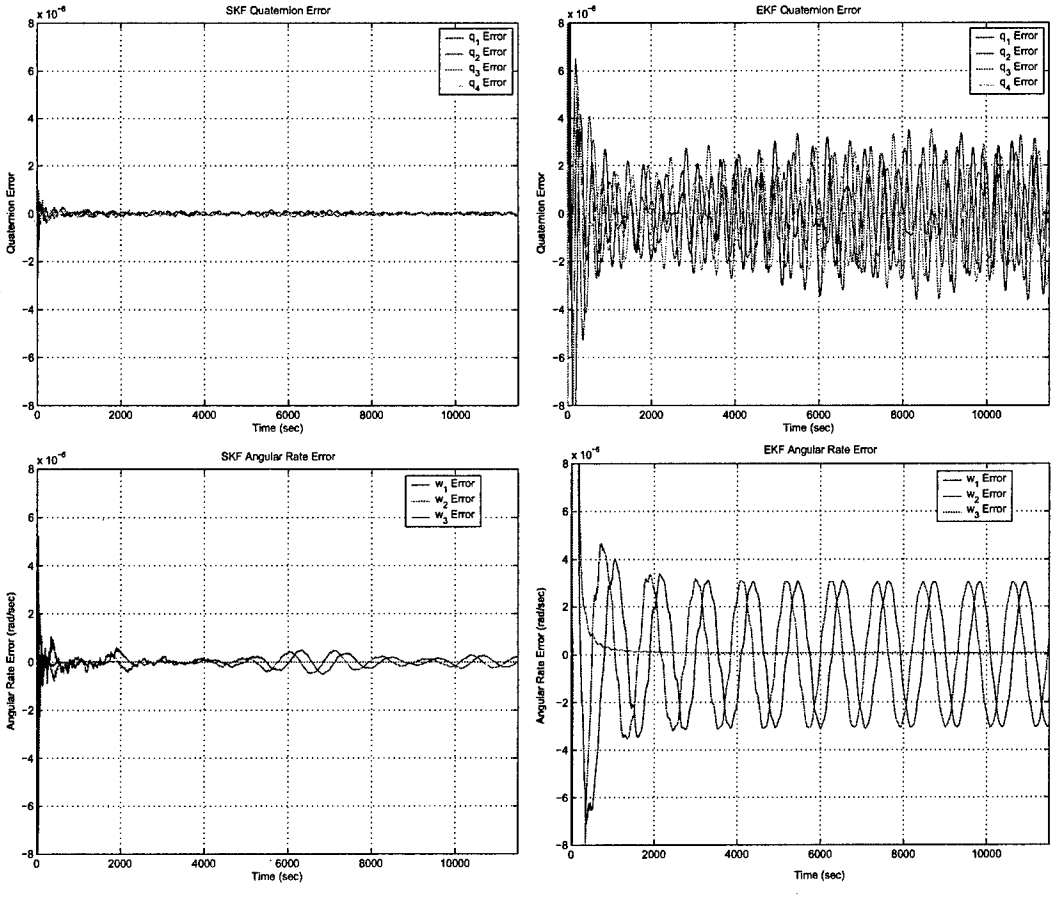

Figure 3: SKF Versus EKF State Estimation Error

The contrast in kinematic and dynamic estimation performance is highlighted using a logarithmic scale for the error values in Figure 4. Remarkably, the SKF state error is one order of magnitude smaller than the EKF state error in the steady

state.

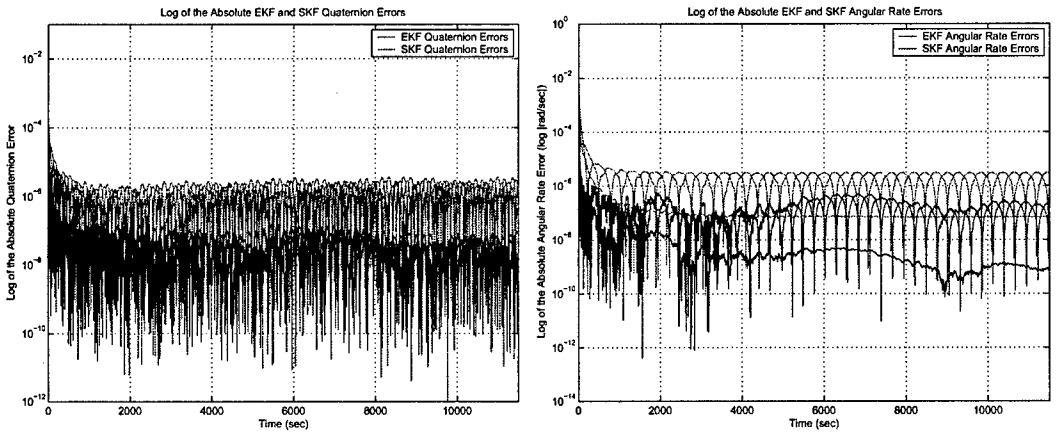

Figure 4: SKF Versus EKF Log State Estimation Error

As hypothesized, the SKF preserves constants of motion to a much higher degree of accuracy than the EKF. The SKF produced rotational energy error two orders of magnitude smaller than the EKF, and angular momentum errors one order of magnitude smaller than the EKF. These results are presented in Figure 5.

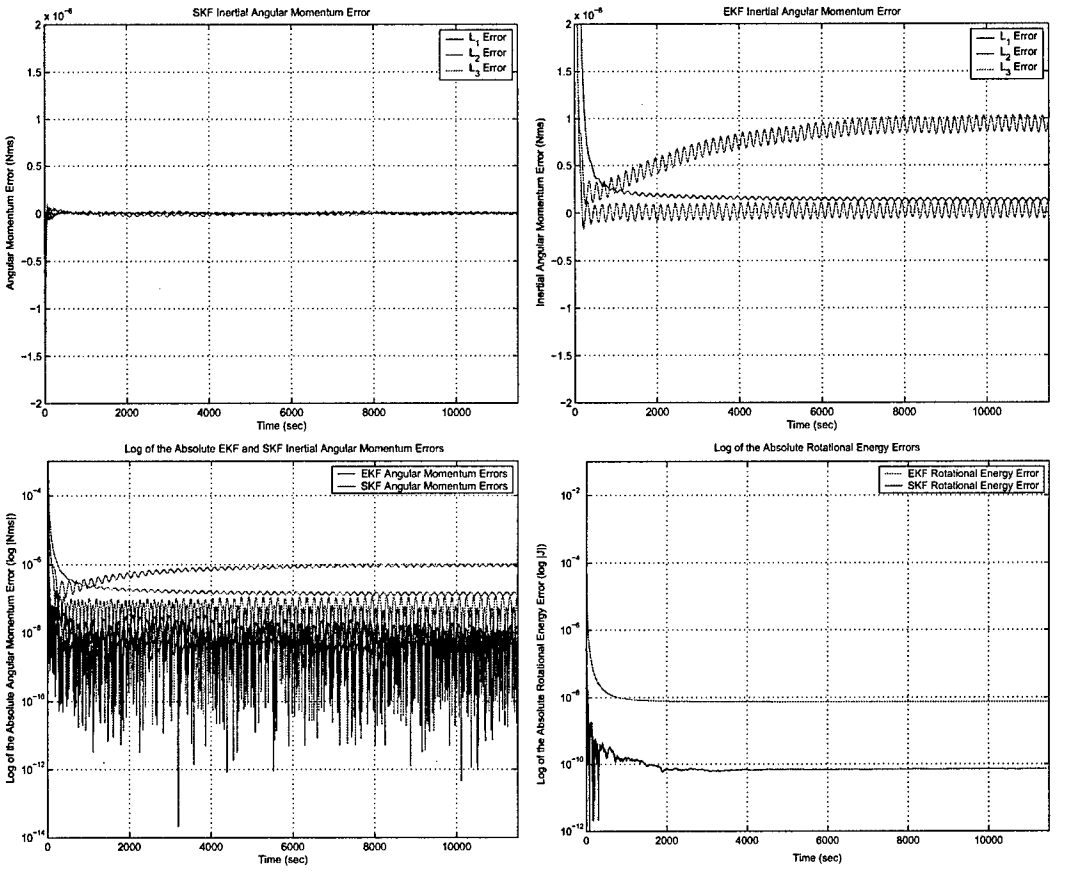

Figure 5: SKF Versus EKF Conserved Values Error

The SKF's better steady-state accuracy and conservation of constants of motion were observed throughout the simulations conducted. Only by reducing the EKF timestep by an order of magnitude in this case was it able to match the steady-state performance of the SKF. In general, the filters' performances converged as the number of timesteps per observation was increased.

CONCLUSIONS

A novel method for efficient high-accuracy satellite attitude estimation based on symplectic numerical methods has been presented. The application of a symplectic integration method to the EKF algorithm outperformed the standard EKF in the presence of nonlinearity and low measurement noise in the 1-D case. Using this result, a six-state SKF was developed for satellite attitude estimation. Numerous small satellite simulations were conducted and the SKF demonstrated orders of magnitude improvement in state accuracy and preservation of constants of motion over the EKF. Based on these results, there appears to be a clear advantage to using the SKF in place of the EKF onboard small satellites that do not have the computa-

tional capacity to accommodate increased model evaluations, especially those with properties modeled above (namely, gyroless agile small satellites with high-accuracy attitude observation devices).

ACKNOWLEDGEMENT

The authors would like to thank the Marshall Aid Commemoration Commission for its generous support via the Marshall Scholarship, and Dr. Yoshi Hashida of the Surrey Satellite Technologies, Ltd. (SSTL) ADCS team for his time, insight, and technical assistance, which proved invaluable throughout the research effort.

References

[1] Markiewicz, D. W., "Survey on Symplectic Integrators," Tech. rep., University of California at Berkley, Spring 1999.

[2] Leimkuhler, B. and Reich, S., *Simulating Hamiltonian Dynamics*, Cambridge Monographs on Applied and Computational Mathematics, Cambridge University Press, Cambridge, 2004.

[3] Channell, P. J. and Scovel, C., "Symplectic Integration of Hamiltonian Systems," *Nonlinearity*, Vol. 3, No. 2, 1990, pp. 231–259.

[4] Hayes, W., "A Brief Survey of Issues Relating to the Reliability of Simulation of the Large Gravitational N-body Problem," Tech. rep., University of Toronto, June 1996.

[5] Mikkola, S., Palmer, P., and Hashida, Y., "A Symplectic Orbital Estimator for Direct Tracking on Satellites," *Journal of Astronautical Sciences*, Vol. 48, No. 1, 1999, pp. 109–125.

[6] Palmer, P., Mikkolla, S., and Hashida, Y., "A Simple High Accuracy Integrator for Spacecraft Attitude Systems," *AIAA Guidance, Navigation, and Control Conference*, Providence, Rhode Island, 2004.

[7] Fiares, J. D. and Burden, R., *Numerical Methods*, Thomson Learning, Pacific Grove, 3rd ed., 2003.

[8] Athans, M., Wishner, R. P., and Bertolini, A., "Suboptimal State Estimation for Continuous-Time Nonlinear Systems from Discrete Noisy Measurements," *IEEE Transactions on Automatic Control*, Vol. AC-13, No. 5, 1968, pp. 504–514.

[9] Bellaire, R. L., *Nonlinear Estimation with Applications to Target Tracking*, Ph.D. thesis, Georgia Institute of Technology, 1996.

[10] Julier, S., Uhlmann, J., and Durrant-Whyte, H. F., "A New Method for the Nonlinear Transformation of Means and Covariances in Filters and Estimators," *IEEE Transactions on Automatic Control*, Vol. 45, No. 3, 2000, pp. 477–482.

[11] Vallado, D. A., *Fundamentals of Astrodynamics and Applications*, Microcosm Press, London, 2nd ed., 2001.

[12] Palmer, P. L. and Mikkola, S., "High Precision Integration Methods for Attitude Modelling," Tech. rep., Surrey Space Centre, 2004.

[13] Palmer, P. L. and Mikkola, S., "On the Integration of the Spacecraft Attitude Equations," Tech. rep., Surrey Space Centre, 2004.

[14] Hashida, Y., "ADCS for Future UoSat Standard Platform: Surrey Satellite Technology Limited Internal Technical Note," Tech. rep., Surrey Satellite Technology Limited, 2004.

[15] Hashida, Y., "Simplified Attitude Estimator," 2005, Simplified Surrey Satellite Technology Limited 6-State EKF Flight Software.

[16] Farrell, J. L., "Attitude Determination by Kalman Filtering," *Automatica*, Vol. 6, No. 5, 1970, pp. 419–430.

[17] Steyn, W. H., *A Multi-mode Attitude Determination and Control System for Small Satellites*, Ph.D. thesis, University of Stellenbosch, 1995.

[18] Hashida, Y., "Quaternion Derivation," Tech. rep., Surrey Satellite Technology Limited, 2004.

[19] Wertz, J. R., editor, *Spacecraft Attitude Determination and Control*, Kluwer Academic Publishers, London, 1978.

[20] Yoshida, H., "Symplectic Integrators for Hamiltonian Systems: Basic Theory," *Chaos, Resonance, and Collective Dynamical Phenomena in the Solar System*, edited by S. Ferraz-Mello, International Astronomical Union, 1992, pp. 407–411.

[21] Mikkola, S., "Numerical Celestial Mechanics," Tech. rep.

[22] Lefferts, E. J., Markley, F. L., and Shuster, M. D., "Kalman Filtering for Spacecraft Attitude Estimation," *Journal of Guidance, Control, and Dynamics*, Vol. 5, No. 5, 1982, pp. 417–429.

[23] Hale, M., "Kalman Filtering and the Attitude Determination and Control Task," Tech. rep., U.S. Air Force Academy, 2004.

[24] Hashida, Y., "RapidEye ADCS Algorithm Specification Revision 1," Tech. rep., Surrey Satellite Technology Limited, 2004.

[25] Visser, B., "Falcon Sat-3 Qualification Model (QM) Thermal-Vacuum, Vibration Test, and Mass Properties Measurement Test Report," Tech. rep., Space Systems Research Center, 2005.

[26] Jorgensen, J. L., Denver, T., Betto, M., and Van den Braembussche, P., "The PROBA Satellite Star Tracker Performance," *4th IAA Symposium on Small Satellites for Earth Observation*, Berlin, Germany, 2003.

[27] Wertz, J. R. and Larson, W. J., editors, *Space Mission Analysis and Design*, Space Technology Series, Microcosm Press and Kluwer Academic Publishers, London, 3rd ed., 1999.

[28] Bate, R. R., Mueller, D. D., and White, J. E., *Fundamentals of Astrodynamics*, Dover Publications, Inc., New York, 1971.

From RS2: Leveraging COTS Hardware for Rapid Design and Development of Small Satellites at the USAF Academy

Cristin Anne Smith (USAFA)

View/Download: Presentation | Paper

Abstract:

The purpose of the United States Air Force Academy (USAFA) Space Systems Research Program is to give cadets the opportunity to "learn space by doing space" while also providing an orbiting platform for Air Force and Department of Defense (DoD) science experiments as FalconSAT-3 is designed to do. This paper describes small satellite programs at the U.S. Air Force Academy's Space Systems Research Center. FalconSAT- 2 and FalconSAT-3 are student-built small satellites that provide low-cost access to space for DoD space research & development payloads as well as platforms for student experiments. Rapid, low-cost design is achieved by leveraging Commercial Off-the- Shelf (COTS) hardware to the greatest extent possible. FalconsSAT-2, still searching for an alternate launch opportunity, was the first to demonstrate the use of COTS modules for this use. FalconSAT-3, scheduled to be launched in 2006, recently completed critical design and built upon the successful FalconSAT-2 experience to develop an even more capable spacecraft bus. By using the off-the-shelf equipment, student involvement in satellite and mission design has been accelerated and provided the capability to challenge students This paper is declared a work of the U.S. Government and is not subject to copyright protection in the United States. through more intense participation over the years. Realizing the rapid turnover and extended commitments of students in a senior undergraduate program, there is a delicate balance to be found; one between comprehensive mission and satellite design requirements, and adequate experience in a multi-million dollar, real world space program. The development of the FalconSAT program will first be described in the context of the progress made, followed by a more detailed discussion of the COTS hardware for more efficient development of small student satellites as simple payload platforms for educational and technological purposes.

REPORT DOCUMENTATION PAGE

Form Approved
OMB No. 0704-0188

1. AGENCY USE ONLY *(Leave blank)*	2. REPORT DATE	3. REPORT TYPE AND DATES COVERED
	20.Jan.06	MAJOR REPORT

4. TITLE AND SUBTITLE
SYMPLECTIC ATTITUDE ESTIMATION FOR SMALL SATELLITES.

5. FUNDING NUMBERS

6. AUTHOR(S)
2D LT VALPIANI JAMES M

7. PERFORMING ORGANIZATION NAME(S) AND ADDRESS(ES)
UNIVERSITY OF SURREY

8. PERFORMING ORGANIZATION REPORT NUMBER
CI04-1729

9. SPONSORING/MONITORING AGENCY NAME(S) AND ADDRESS(ES)
THE DEPARTMENT OF THE AIR FORCE
AFIT/CIA, BLDG 125
2950 P STREET
WPAFB OH 45433

10. SPONSORING/MONITORING AGENCY REPORT NUMBER

11. SUPPLEMENTARY NOTES

12a. DISTRIBUTION AVAILABILITY STATEMENT
Unlimited distribution
In Accordance With AFI 35-205/AFIT Sup 1

DISTRIBUTION STATEMENT A
Approved for Public Release
Distribution Unlimited

12b. DISTRIBUTION CODE

13. ABSTRACT *(Maximum 200 words)*

14. SUBJECT TERMS

15. NUMBER OF PAGES
19

16. PRICE CODE

17. SECURITY CLASSIFICATION OF REPORT	18. SECURITY CLASSIFICATION OF THIS PAGE	19. SECURITY CLASSIFICATION OF ABSTRACT	20. LIMITATION OF ABSTRACT